

# Particle ID performance of Liquid Argon TPC

J-PARC T32 collaboration

---

## Abstract

This paper describes a study of particle identification performance of liquid Argon TPC (LArTPC) detector using well-defined charged particles (pions, kaons, and protons) with momentum of 800 MeV/c obtained at J-PARC K1.1Br beamline.

We have build a LArTPC detector with fiducial mass of 150 kg, and injected the beam particle

*Keywords:*

---

## **1. Introduction**

Refer [1] for hardware/beam line description

## 2. Data Quality

### 2.1. Collected Data

Table 1 shows list of the collected data while Oct/2010 Run. 800 MeV/c pion is expected to pass-through the detector as MIP, and have uniform energy deposition to all the TPC channels. So this data set is very useful for calibrating the detector response (See section xxx). 800 MeV/c proton stops after 15 cm of flight distance inside the TPC fiducial volume with relatively large  $dE/dx$ . So we use the proton data set for validation of the detector response at high  $dE/dx$  region(See section xxx). We have collected three different Kaon data by varying thickness of the degrader. 540, 630, 680 MeV/c corresponds to the momentum degraded by 2 lead glass, 1 lead glass + 1 lead block, and 1 lead glass, respectively, and such Kaon stops after 10 cm, 50 cm, and 65 cm of flight distance inside TPC fiducial volume.

Figure 1 shows an 2D display of typical event taken with 800 MeV/c electron trigger. Horizontal axis corresponds to TPC channel number and zero means most upper stream strip. Since strip pitch is 1 cm, this is equivalent to distance from beam injection point in cm. Vertical axis corresponds to electron drift time in  $\mu s$  and  $t=0$  means trigger timing. In this TPC, anode and cathode is located at top and bottom of the detector, respectively,  $t=0$  means energy deposition at anode and longer drift time means energy deposition in lower height. With 200 V/cm of electric field, drift velocity is about 0.8 m/ms. So drift of full detector (40 cm) takes 500  $\mu s$ . Color strength of the plot corresponds to the TPC signal pulse height in ADC counts which is roughly proportional to  $dE/dx$  of the track. In this event, triggered electron can be clearly seen center of the detector as an electromagnetic shower while there are two other particles accidentally overlapped with the triggered electron. Track at  $t=100 \mu s$  is considered as a proton which stops after 15 cm of flight distance and has large  $dE/dx$  around the stopped point. Track at  $t=400 \mu s$  is considered as a pion which passes-through the detector and has uniform  $dE/dx$  over the TPC channels. This event already gives us some idea for how good the particle identification performance of the LArTPC is.

Figure 2 shows a typical  $K \rightarrow \mu\nu$  like event. We can clearly identify a kink of the track at 60 cm which is considered as stopped point of Kaon and it decays to

Energy deposition of the track is about MIP at the injection point and gradually increase towards the stopped point at 60 cm.

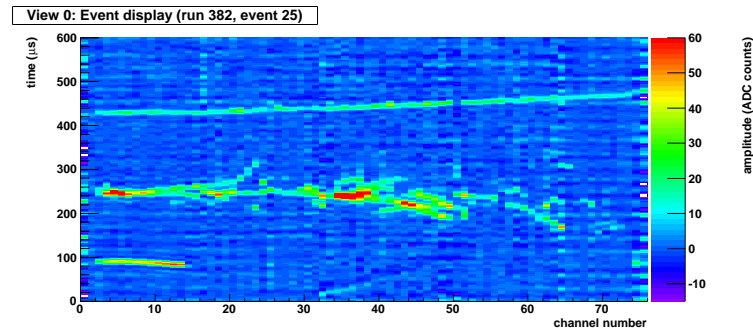


Figure 1: Event display of 800 MeV/ $c$  electron triggered event. Accidentally overlapped with a proton and a pion.

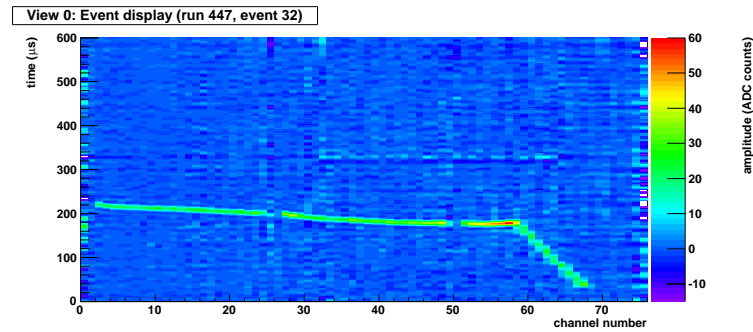


Figure 2: Event display of Kaon 630 MeV/ $c$  triggered event

Table 1: List of collected data

Particle	Momentum (MeV/c)	Number of Events
Pion	800	3,000
Proton	800	1,500
Kaon	540 (2LG)	7,000
Kaon	630 (1LG+1LB)	40,000
Kaon	680 (1LB)	35,000
electron	800	2,500
electron	200	10,000
pion	200	10,000

## 2.2. Beam Quality(Purity)

We have several beam counters to identify beam particles event by event (see Fig3). Using this when taking data, we can get data of interest selectively. The following describe how to identify beam particles with the typical data including  $K^+$ ,  $\pi^+$ ,  $e^+$ ,  $p$  events, which have the momentum adjusted  $\sim 800\text{MeV}/c$ .

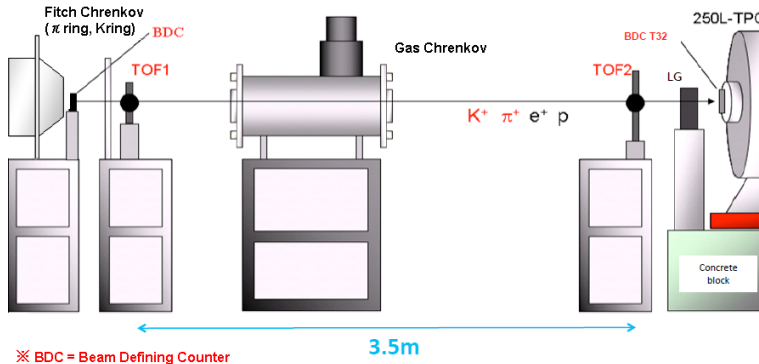


Figure 3: Instruments on K1.1BR Beam Line

Leaded particles to K1.1BR beam line pass the Fitch Cherenkov Counter at first. Fitch Cherenkov Counter can select particles with differences of angle of cherenkov light which they radiate. Figure4 shows the response of the Fitch Cherenkov Counter. The horizontal axis shows the total amount of PMT signal where cherenkov light of  $800\text{MeV}/c \pi$  can be detected. The vertical axis shows that of  $800\text{MeV}/c K$ . Signals are distinctly separated to

three cluster and can be categorized as following.

1.  $\text{FC}(\pi)$  Signal < 1450 &  $\text{FC}(K)$  Signal > 2000
2.  $\text{FC}(\pi)$  Signal < 1450 &  $\text{FC}(K)$  Signal < 2000
3.  $\text{FC}(\pi)$  Signal > 1450 &  $\text{FC}(K)$  Signal < 2000

Apparently, particles within the region 1 are  $K^+$  candidates. Particles within region 2 are  $p$  candidates because  $800\text{MeV}/c$   $p$  is impossible to radiate cherenkov light. Particles within region 3 are  $\pi^+$  or  $e^+$  candidates because their angle of cherenkov light are almost same level.

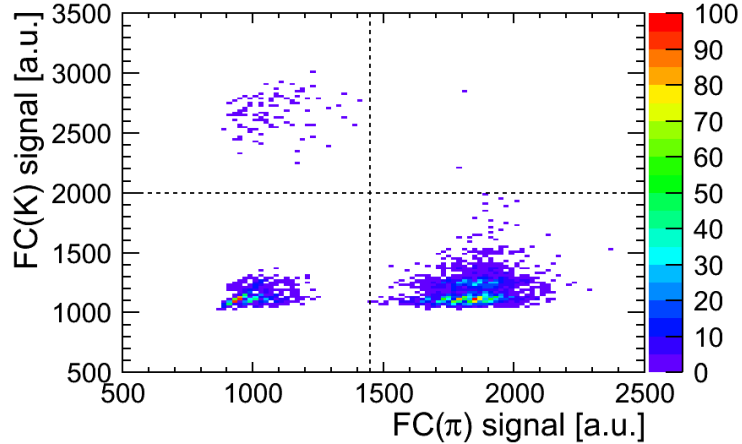


Figure 4: Fitch Cherenkov Counter

Gas Cherenkov Counter can select  $e^+$  from the other particles because only  $e^+$  can radiate cherenkov light at the refractive index of this gas. Figure 5 shows the response of the Gas Cherenkov Counter. The horizontal axis shows the PMT signal of the Gas Cherenkov Counter. The vertical axis shows the number of events. Fitting the pedestal with Gaussian function, the events larger than the value added  $\sim 3.5\sigma$  to the mean of the pedestal is  $e^+$  candidates. In this case, GC signal is required more than 104.7 to be  $e^+$

particle	$e^+$	$\pi^+$	$K^+$	$p$
Mass(MeV)	0.511	139.57	493.68	938.27
Time of Flight(ns)	11.67	11.84	13.71	17.98

Table 2: Time of flight of each particle

candidates.

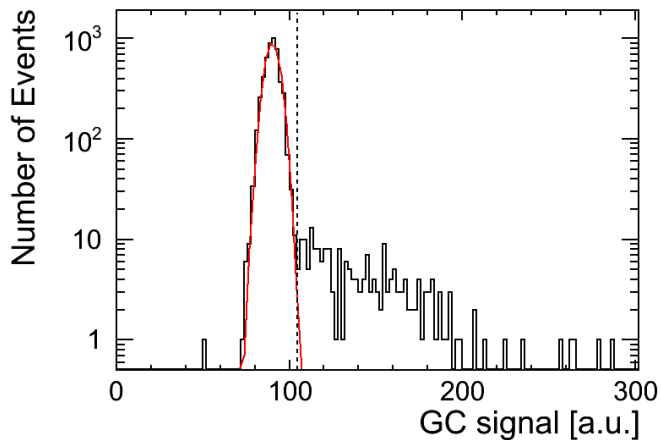


Figure 5: Gas Cherenkov Counter

There are two TOF Counters which has  $\sim 200$  ps resolution 3.5m apart, and each particle can be selected with the difference of time of flight between them. Following table2 is calculated time of flight when each 800MeV/c particle passes two counters. As this table shows,  $e^+$  and  $\pi^+$  cannot selected because the difference of time of flight is too short for the TOF resolution.

Figure6 shows response of the TOF Counters. The horizontal axis shows the time of flight between TOF1 and TOF2 Counter. The vertical axis shows the number of events. Signals have clearly divided three structures. From table2, in ascending order of time of flight the first structure include  $e^+$  or  $\pi^+$  candidates, and the second structure include  $K^+$  candidates, and the third structure include  $p$  candidates. The cut value to separate the first structure and the second structure is  $\sim 4.5\sigma$  (in this case, the value is set 13.15ns), and because the second structure and the third structure is clearly separated, the

cut value to select them is set 16.47ns fully apart from the second structure.

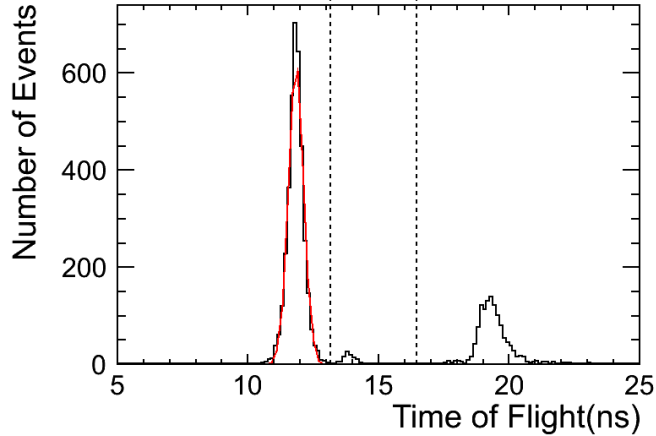


Figure 6: TOF Counter

$K^+$  can selected very efficiently with Fitch Cherenkov Counter, so we require the condition FC Signal( $K$ ) is more than 2000 to get  $K^+$  events in taking data. Figure7 shows response of the TOF Counters before and after above cut. The histogram which filled with black is what is after cut. This figure shows we can get high-purity  $K^+$  samples with this condition.

Particles which satisfy all conditions for the same candidate are identified themselves, and the others are defined ‘uncertain’ particles. Herewith, we can identify beam particles with high purity before injection to 250L detector. Table2.2 shows the beam components of the data used for analysis.

Run 52,55,59 and 60 are the data required the condition FC Signal( $K$ ) is more than 2000 in taking data to get  $K^+$  events. Therefore the selection of  $K^+$  on the analysis required by only TOF, that is, time of flight is 12.72~17.72ns, and the others are defined *uncertain*. As table2.2 shows, these data is almost occupied  $K^+$  events and the ratio is  $\sim 99.2\%$  on average.

### 2.3. Beam Energy

#### 2.3.1. Kaon energy

Time resolution of TOF counters is not enough to determine Kaon beam energy. Kaon beam energy is estimated by comparing decay point distribu-

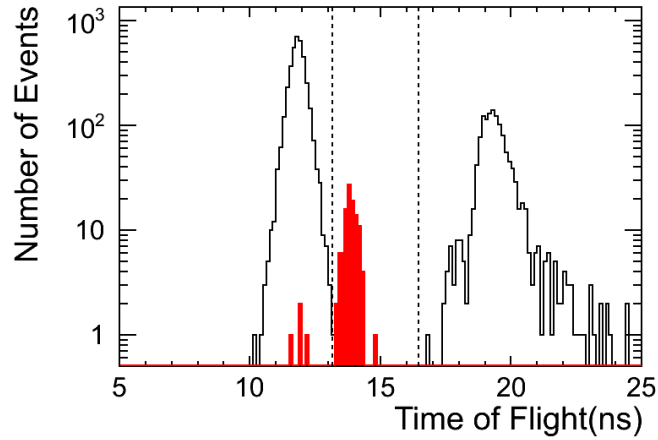


Figure 7: TOF Counter after  $K^+$  selection

Run Number	$e^+$	$\pi^+$	$K^+$	$p$	<i>uncertain</i>	Number of Events
42	68	1617	27	232	5	1949
48	128	1594	78	126	11	1937
49	0	341	0	1146	12	1499
52	0	0	3169	0	34	3203
55	0	0	8534	0	66	8600
59	0	0	5900	0	50	5950
60	0	0	1899	0	13	1912

Table 3: Beam components of data used for analysis

tion of data and MC simulation as described in section 6.8.1.

### 2.3.2. Proton energy

Since proton mass is relatively heavy, proton energy is determined by TOF counters information. Figure 8 shows  $\Delta\text{TOF}$  distribution of TOF counters. Figure 9 shows proton momentum estimated by TOF counters information.

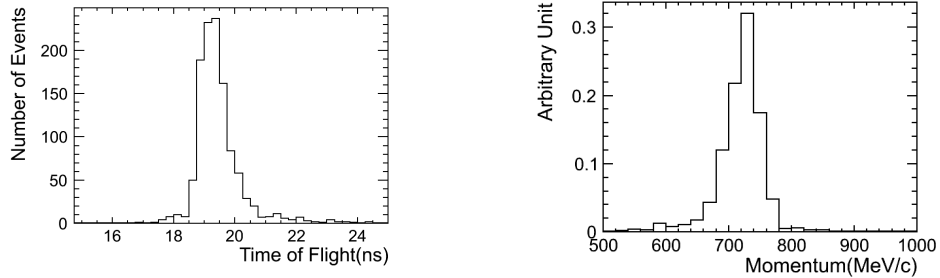


Figure 8:  $\Delta\text{TOF}$  distribution of TOF counters with proton data

Figure 9: proton momentum estimated by  $\Delta\text{TOF}$  of TOF counters information

### 2.4. Beam Position

We measured beam profile in front of 250LAr TPC beam window by using plastic scintillation counters. Figure 10 shows beam profile result.

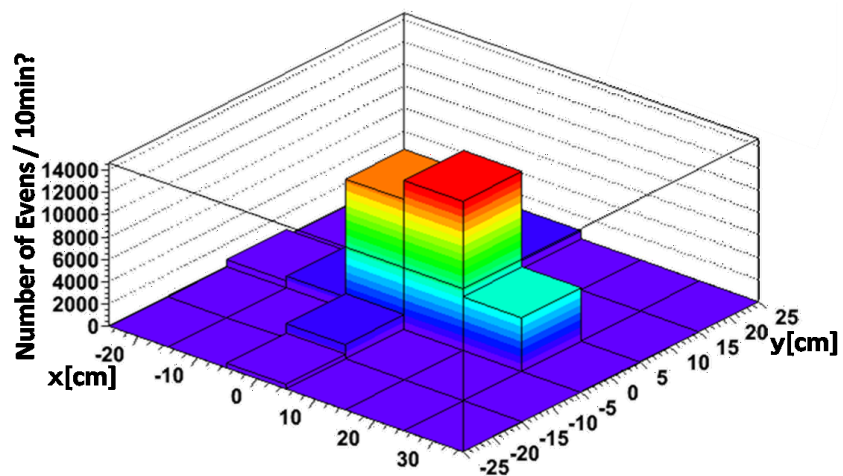


Figure 10: Beam profile on the front of 250LAr TPC

### **3. Software Framework**

Qscan is a general purpose software package for LArTPC analysis(reference) which provides,

- event reconstruction: noise reduction, hit finding, clustering, and tracking...
- event simulation: GEANT VMC with ROOT geometry, ionization electron recombination, drift, digitization...
- event visualization: display raw data waveform and reconstructed quantities

## 4. Event Reconstruction

### 4.1. Noise Reduction

Figure 12 shows raw waveform of the TPC signal before applying any noise reduction. Two waveforms shown in this plot are channel 13 and 37 in Figure 1 which are roughly proton stopped point and electron shower maximum point, respectively. Signal-to-noise ratio for this particular case is poor and pion signal which is supposed to be  $t=400 \mu\text{s}$  is almost hidden by the noise. While time width of TPC signal is few  $\mu\text{s}$  which is determined by drift time between anode and anode-grid, dominant noise component looks higher frequency. To reduce such noises, we have applied FFT (Fast Fourier Transformation) filter to cut the high frequency component. Figure ?? shows amplitude as a function of frequency for the same event. This clearly shows dominant noise component with  $> 200 \text{ kHz}$  has good separation with signal component ( $< 100 \text{ kHz}$ ). Figure 13 shows the waveform after removing high frequency ( $> 80 \text{ kHz}$ ) component by the FFT filter. Signal-to-noise ratio is dramatically improved. On the other hand, we expect certain bias to the signal charge measurement by this filter, and it will be discussed in Section X.

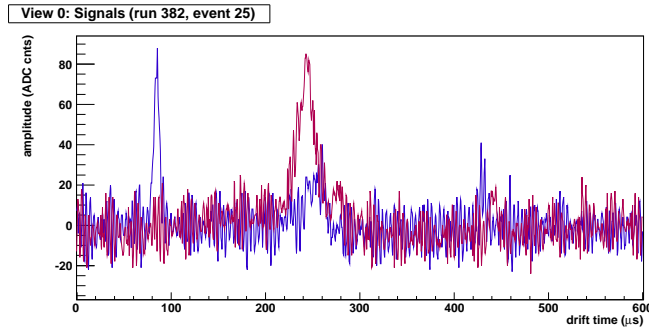


Figure 11: TPC raw signal waveform for "Textbook" event channel 13 and 37.

### 4.2. Hit Finding/Clustering

After noise reduction we find signal hits and create clusters associated to single tracks. Hit is defined as bump over given threshold in a channel. After finding all hits in an event, we construct cluster by merging adjacent hits. The example of hit finding and clustering is shown in Fig 14, which

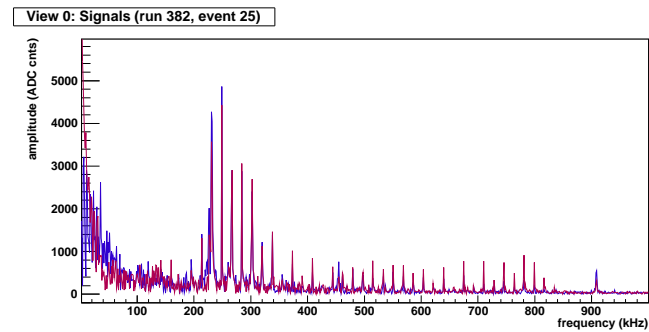


Figure 12: FFT frequency amplitude distribution

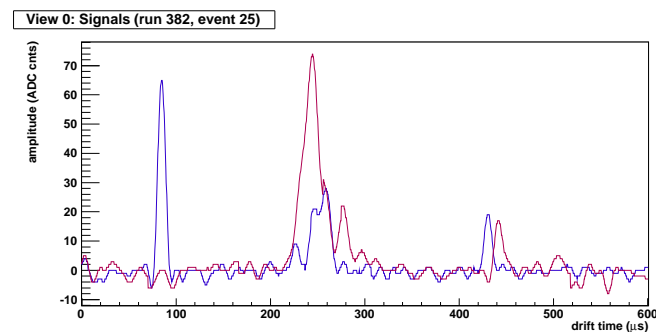


Figure 13: TPC signal waveform after cutting the frequency > 80 kHz.

indicates reasonable hit and cluster findings. Threshold of hit finding is 6 ADC counts, which is about  $2.5\sigma$  from typical data noise level (as shown in Fig 12) and keeping more than 99% of Kaon hit finding efficiency from simulation. ADC count distribution is fitted by step function plus Gaussian to estimate the charge of hit in  $\text{ADC} \times \mu\text{s}$  unit. Fitting  $\chi^2 < 3$  and  $2.5 < (\text{time width of hit}) < 8 \mu\text{s}$  are required to remove noise hits further.

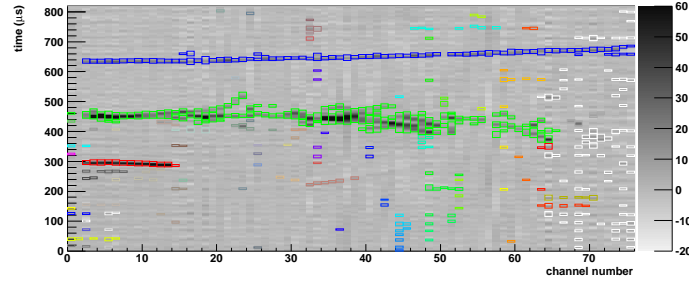


Figure 14: Example of hit finding and clustering. A colored box corresponds to a hit and colors represent different clusters.

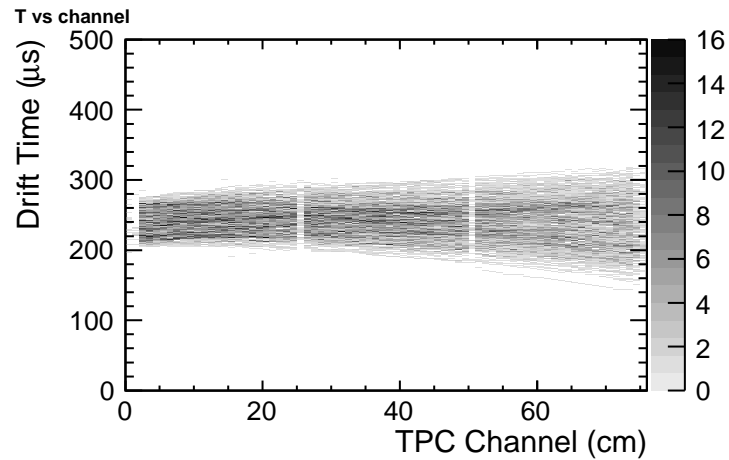


Figure 15: 800 MeV/c pion sample

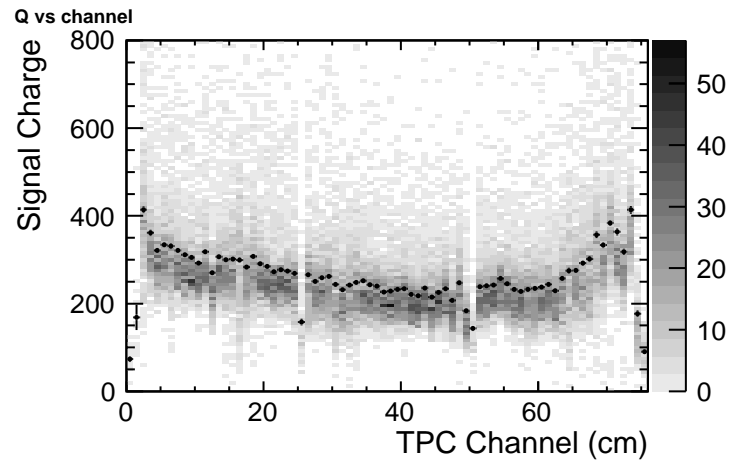


Figure 16: 800 MeV/c pion average hit charge

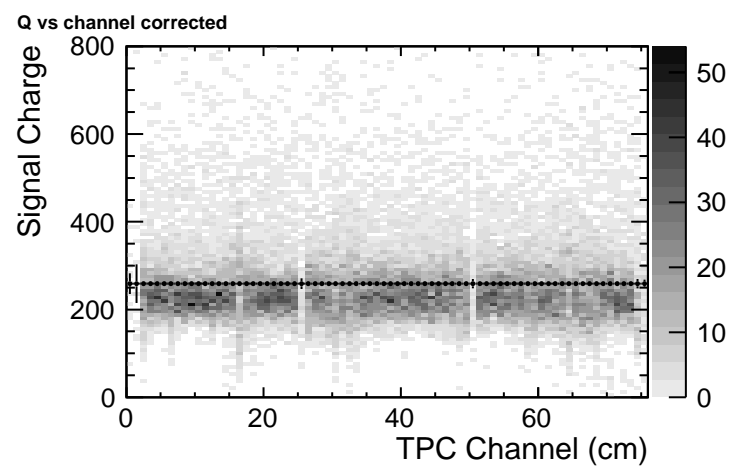


Figure 17: 800 MeV/c pion average hit charge after calibration

### 4.3. Stopped Point Finding

#### 4.3.1. Proton

Figure 18 shows typical event of proton. Proton has simple structure of events because proton doesn't decay any particles. Therefore, it is easy to define stopped point. We define the hit which has the maximum channel number as stopped point. However, it should noted that stopped point include fake hit in a proportion because of the influence of cross talk as described in section 6.6.

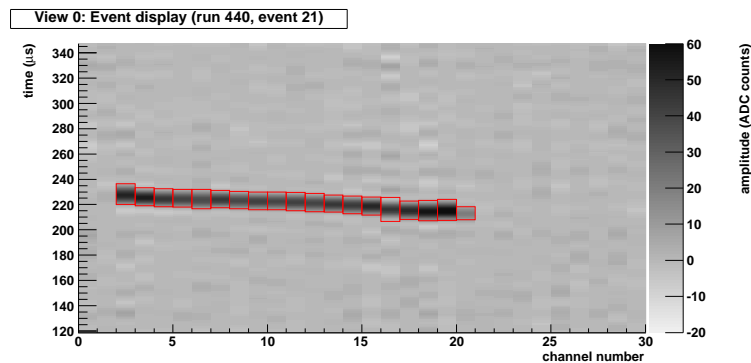


Figure 18: Typical Event Display of Proton

#### 4.4. Stopped Kaon

Hough transform was invented for machine analysis of bubble chamber photographs by Paul.V.C.Hough.[6] We find straight lines using hough method , and find Kaon stopped point from the intersection of straight lines. Figure 19 shows hit map like a Kaon track. One point in the X-Y space can be transformed into sinusoidal curve in the  $\rho$ - $\theta$  space. Figure 20 shows sinusoidal curves in all points. And, we find the straight line associated with the largest number of points by choosing the most dense point in  $\rho$ - $\theta$  space. Next , the sinusoidal curves of the hits associated with frist straight line are removed from figure 20. Figure 21 shows sinusoidal curves after the hits associated with frist straight line removed. We find second straight line using the same procedure. This procedure is repeated until there are less than three points. Figure 22 shows the two straight lines found by hough transform mehodt.

Kaon stopped point in the liquid argon detector defined as charge maximum point around the intersection of some lines.

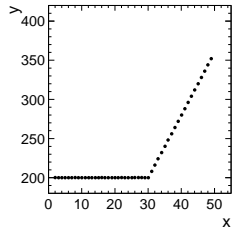


Figure 19: Hit map like a Kaon track

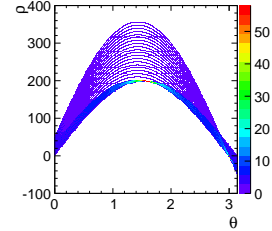


Figure 20: Sinusoidal curves getting form all hough transformed points of Figure 19

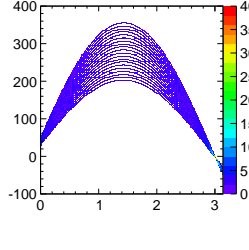
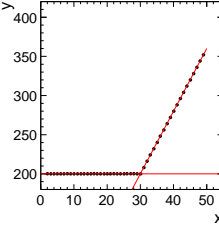


Figure 21: Sinusoidal curves removed the points associated with first straight line from figure 20

Figure 22: Two lines found with hough transform method



#### 4.4.1. Chi<sup>2</sup> method

$\chi^2$  method is the algorithm that search the point of rapidly increasing fit'  $\chi^2$  and the point defined as the stopped point. Because the charged particle coming from upstream of beam line , track reconstruction is started from minimum channel to the maximum channel of the cluster.

Figure 23 shows hit map like a Kaon track. We start fitting with straight line from minimum channel to maximum channel. Figure 24 shows range vs fit'  $\chi^2$  distribution. As it can be noticed for figure 24,  $\chi^2$  is increased rapidly if the straight line is strayed out. Then , we search the strayed point from the straight line by setting reasonable threshold and draw from minimum channel to the strayed point. This procedure is done from maximum channel to minimum channel in the same way. And we draw from maximum channel to

the strayed point. Kaon stopped point in the liquid argon detector defined as charge maximum point around the intersection of two lines.

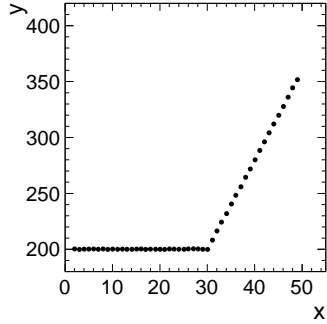


Figure 23: hit map like a Kaon track

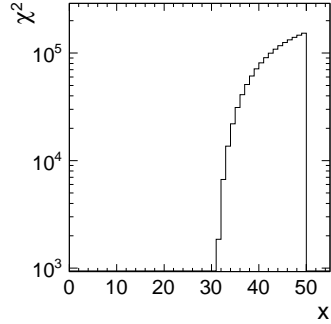


Figure 24: range vs  $\chi^2$  distribution

#### 4.4.2. BS method

In the  $\chi^2$  method , we can't find Kaon stopped point in the case of backward decay. Then , we find Kaon stopped point using BS method.

BS method is concept that the Kaon stopped point defined as lightmost channel in the case of backward decay. we descript below how the track defined as backward decay.  $N_1$  is defined as Number of cluster hits found by the clustering. Stopped point finding is started from minimum channel. We search for the closet timing hit in next channel from current channel hit. Then , we repeat this procedure until maximum channel and count the number of selected hit information( $N_2$ ). In the case of backward decay ,  $N_1$  is larger than  $N_2$ . So , we set reasonable threhold of the difference between  $N_1$  and  $N_2$  , and if the  $N_1 > N_2$  is over the threshold , the track is defined as backward decay. In the case of backward decay , we defined charge maximum point around the maximum channel as the stopped point.

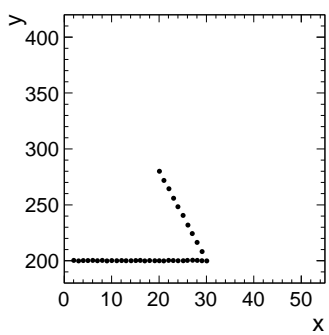


Figure 25: hit map like a Kaon track

## 5. Liquid Argon Purity

Attenuation of the drift electron depends on purity of LAr since electronegative impurities capture it [5]. Thus we need to apply correction to TPC signal charge depends on the drift time. We use cosmic ray sample triggered by inner PMT at off-beam timing for measuring the LAr purity, and use this to correct the beam data. Figure 26 shows an event display of typical cosmic muon event across TPC channels. The attenuation of readout charge depending on drift time is clearly seen in the right plot. Readout charge in an event cannot be fitted by exponential because energy deposition follows Landau distribution and charge readout is affected by electric field distortion which is described latter in section ??.

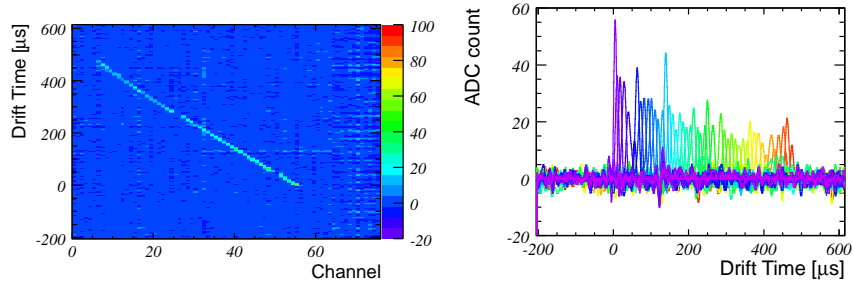


Figure 26: Left: Typical cosmic muon event across TPC channels. Right: Charge deposit as a function of drift time. Colors correspond to different TPC channels.

We select cosmic ray event with more than 20 TPC channels which corresponds to zenith angle of more than  $27^\circ$  and consistent with straight line by  $\chi^2$  fit. Readout charge is corrected for field distortion and projected to beam direction to correct injection angle. We fit readout charge by Landau function in each drift time bin to estimate average charge deposit. Figure 27 shows example of the average readout charge as a function of drift time which is fitted by exponential to obtain drift electron lifetime. Realistic Monte Carlo simulation shows about 13% (TBU) smaller lifetime estimation due to noise, field distortion, and FFT effects. We correct output lifetime from these effects. Figure 28 shows an drift electron lifetime as a function of duration after initial LAr filling. Drift electron lifetime was  $600 \mu\text{s}$  at 60 hours, and  $400 \mu\text{s}$  after 150 hours. The degradation is possibly due to impurity from micro

leak or out-gassing penetrating faster than purification by gas recirculation. But we kept enough drift electron lifetime during data taking period.

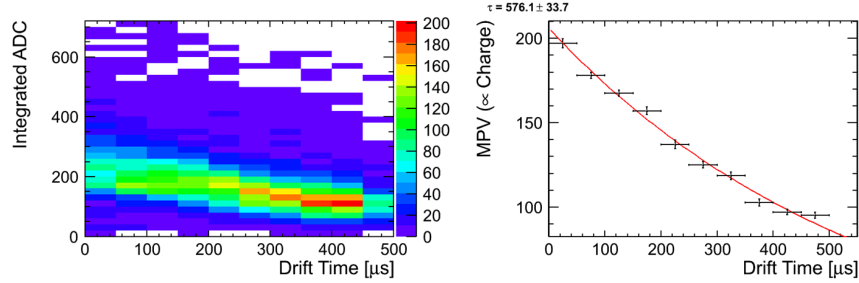


Figure 27: TBU. Left: Readout charge as a function of drift time. Readout charge in each drift time bin is fitted by landau function. Right: Average charge readout as a function of drift time which is fitted by exponential to estimate drift electron lifetime.

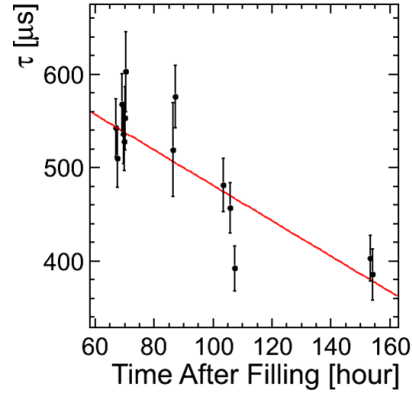


Figure 28: TBU. Drift electron lifetime as a function of duration after initial LAr filling. The lifetime is used to correct the beam data.

## 6. Event Simulation

### 6.1. Geant3, recombination, drift velocity

We use GEANT3 for simulating energy deposition of initial beam particles and secondary particles to LArTPC detector and beamline counters.

we set the maximum step of Geant to 0.5 mm which is enough smaller than the readout pitch of 1 cm. It means charge deposition in one strip is typically simulated with 20 GEANT steps.

We set energy cut-off for soft electron/photon emission to 10 keV which is minimum possible energy can be set in GEANT3. This cut-off is very important for ionization electron recombination.

Recombination of electron and Argon ion depends on the electric field and  $dE/dx$ . We use a measurement in Ref.[3].

$$Q = A \frac{Q_0}{1 + kdE/dx}, A = 0.800, k = 0.486 \quad (1)$$

Velocity of the drift electron depends on the liquid Argon temperature and the electric field. We use a measurement in Ref [4].

- Plot: Geant Geometry, typical track (Tanaka)
- Plot: recombination factor, drift velocity (Tanaka)

### 6.2. Electric Field

Electric field of the TPC field cage We have calculated the electric field using a 2D FEM (Finite Element Method) package [? ].

This field map is used for simulating electron drift.

### 6.3. Drift Electron Diffusion

- Plot: drift simulation (Tanaka)

### 6.4. Preamp Gain Calibration

- Preamp gain vs channel number (Naito)

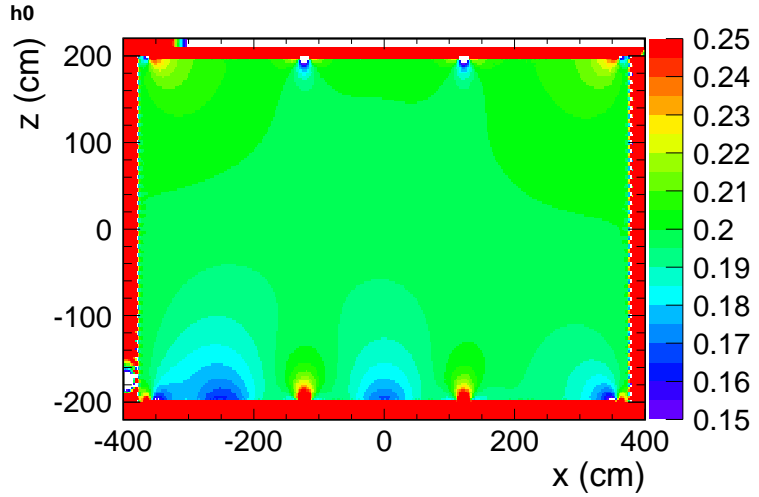


Figure 29: Electric field map obtained from 2D FEM calculation

### 6.5. FFT Noise

There are two kind of noise in the data we obtained, random noise and coherent noise. Random noise is the noise which exists in each anode channel. Coherent noise is in each board. The pseudo noise we implemented in Monte Carlo simulation is composed of random and coherent noise by this reason.

Random noise is generated from FFT(Fast Fourier Transform) distribution of real data. Figure 30 shows an example of FFT distribution.

Coherent noise is generated board by board as the noise scale in the real data we obtained. The noise scale is defined as a root mean square of pedestal, minimun noise scale is about 3 and maximum noise scale is about 10 in the data.

The ratio of random and coherent noise is 1:1 as equation 2. Figure 31 shows real data noise and Fig.32 shows pseudo noise we implemeted in Monte Carlo simulation.

$$Pseudo\ Noise = \frac{Random\ Noise + Coherent\ Noise}{2} \quad (2)$$

- Plot: simulated event (Nagasaki)

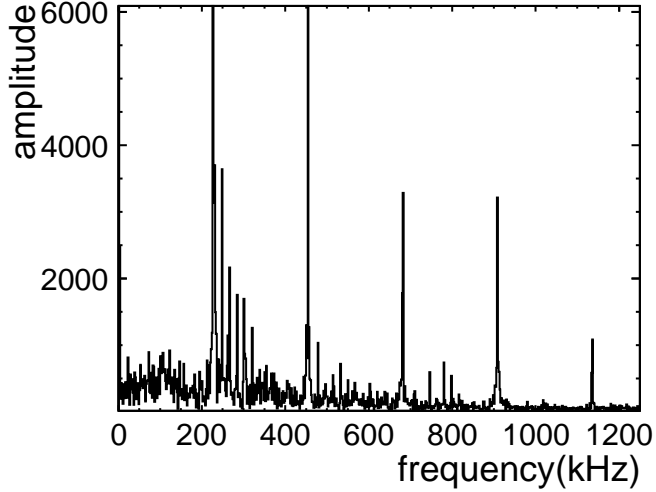


Figure 30: An example distribution of frequency

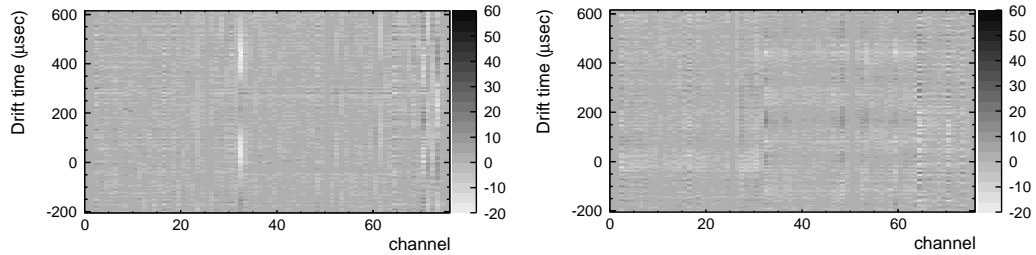


Figure 31: Data noise

Figure 32: Pseudo noise(Noise simulation)

### 6.6. Cross Talk

The distance between anode channels is very short, so the influence of mutual capacitance become large and this capacitive coupling induce cross talk noise. This effect notably appears the channel where the difference of the charge between adjacent channels is large, such as the channel around stopped point of proton. Figure 33 shows the signal wave form of stopped channel and the front channel of typical proton event. The signal wave form of stopped channel is differential form of the one of the front channel. This shape is appeared at channel number 1 which cannot enter drifted ionization electron in electric power lines. These facts show the existence of cross talk. Then, we implement this crosstalk phenomenon in Monte Carlo Simulation

by adding bipolar shape of the signal gaussian shape at adjacent channels. The area of the mountain of cross talk bipolar shape is 10.5% of the area of signal gaussian at each adjacent channel. The value of 10.5% is determined by comparing the distribution of integrated ADC at stopped channel between DATA and MC. Figure 34 shows integrated ADC distribution of stopped channel. Black is DATA and blue is simulation with cross talk red is simulation without cross talk. As this figure shows, DATA and MC with cross talk is good agreement, and the value of 10.5% is reasonable.

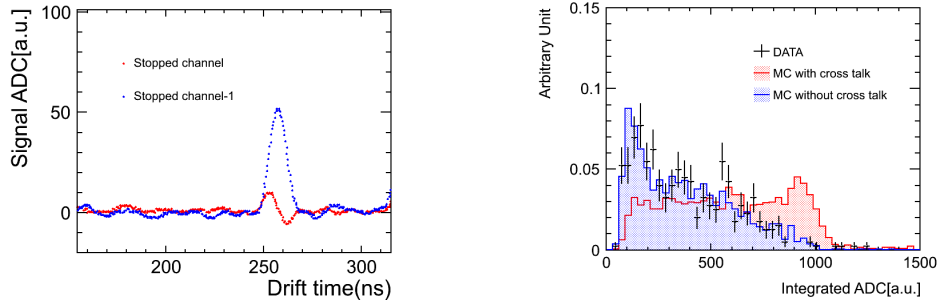


Figure 33: Signal waveform of stopped channel and the front channel

Figure 34: Integrated ADC distribution of stopped channel

- Plot: signal waveform (proton stopped point + 1) (A. Okamoto)
- Plot: simulated event with and without cross talk (A. Okamoto)

### 6.7. Signal and Noise Scale Tuning

- Plot: Landau distribution after the tuning (Tanaka)

### 6.8. Beam energy

We estimated a beam momentum using simple MC simulation. Figure 35 shows MC simulation's geometry. We generate 800MeV/c pencil beam and shoot the beam downstream. Figure 36 shows Kaon and Pion momentum distribution using this MC simulation at BDC. Kaon beam momentum is estimated by the momentum distribution of MC simulation.

#### 6.8.1. Kaon energy

Kaon beam momentum is estimated by the momentum distribution of MC simulation. We change Kaon beam momentum in a range of 700 - 800 MeV/c and search the momentum that decay point distribution of MC simulation is consistent with data one.

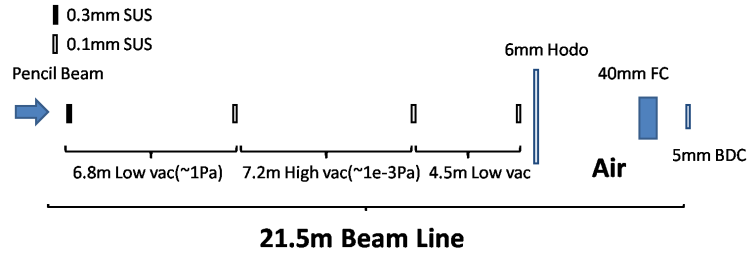


Figure 35: K1.1 Br beam line

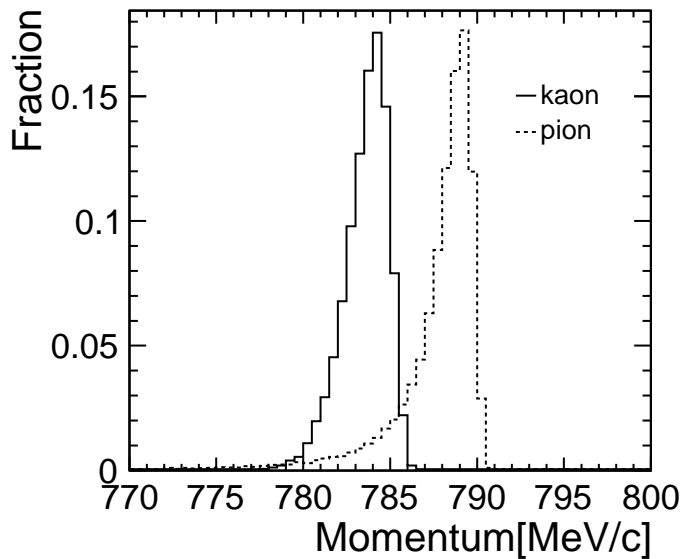


Figure 36: Kaon and Pion momentum distribution at BDC

### 6.8.2. Proton energy

Proton momentum shown in Figure 9 is used as proton beam momentum of MC simulation.

### 6.8.3. Energy deposition in degrader

It is too high energy that Kaon beam stops in the fiducial volume of 250LAr TPC. In order to degrade the beam momentum, some lead glass blocks and a lead brick were inserted in front of 250LAr TPC as degrader. Figure 37 shows energy deposition distribution in degrader.

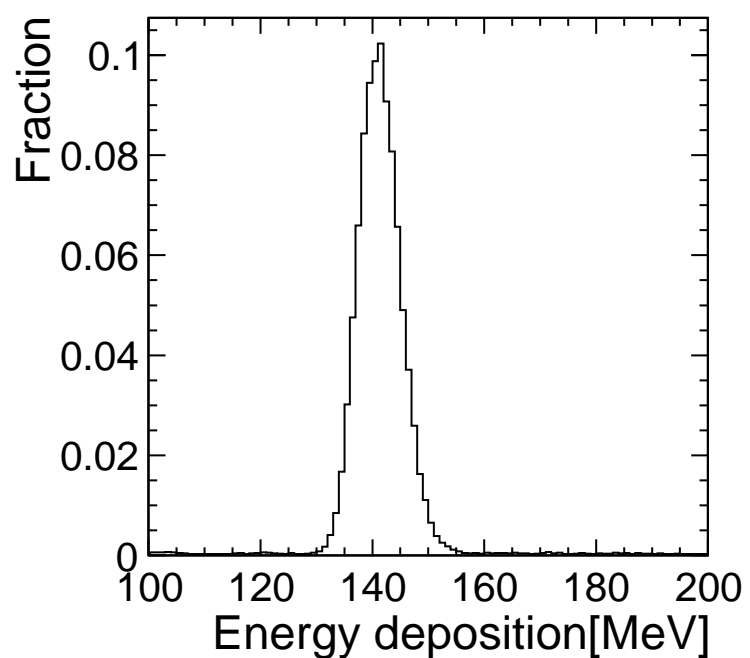


Figure 37: Energy deposition in degrader

## 7. Data- MC Comparison

### 7.1. Through-going Pion

- Plot: Data-MC comparison (Tanaka)

### 7.2. Stopped Proton

When we indicate the validity of charge response in high dE/dx region, proton is good sample due to its simple event structure. At the same time, we verify the recombination factor by proton in this analysis because proton has wide dE/dx range, and this is meaningless if the charge response of MC doesn't agree with that of DATA. Therefore proton is very important in terms of comprehension of charge response.

First, protons are selected by the information of beam counters. Then, proton events are applied following simple selections.

1. The drift time of the hit of the minimum channel number in the cluster is between  $150\mu\text{s} \sim 300\mu\text{s}$ (this time window is signal region).
2. The minimum channel number of hits in the cluster is below 2.
3. The maximum channel number of hits in the cluster is below 60.
4. The total hit number in the cluster is 5 or more.
5. The number of hits which are in the same channel is only one.

We define the events which the number of clusters in the event which passed above selections is only one as good proton events. For good proton events, we compare each parameters of DATA and MC. Figure?? shows the comparison of the distribution of Hit Charge, Hit Sigma, Stopped Channel and Cluster Charge between DATA and MC. Table7.2 shows the comparison of the mean of these distribution.

All four distribution of MC reproduce DATA well. Especially, the agreement of stopped channel distribution indicates the success of the momentum estimation by TOF infomation because where proton stopped depends on

	DATA	MC	DATA/MC ratio
Hit Charge	$607.5 \pm 19.6$	$622.3 \pm 0.8$	$0.9762 \pm 0.0316$
Hit Sigma( $\mu$ s)	$3.838 \pm 0.003$	$3.881 \pm 0.002$	$0.9889 \pm 0.0009$
Stopped Channel	$18.16 \pm 0.20$	$17.72 \pm 0.11$	$1.0247 \pm 0.0132$
Cluster Charge	$9940 \pm 407$	$9735 \pm 59$	$1.0210 \pm 0.0422$

Table 4: Comparison of the mean of four distributions between DATA and MC

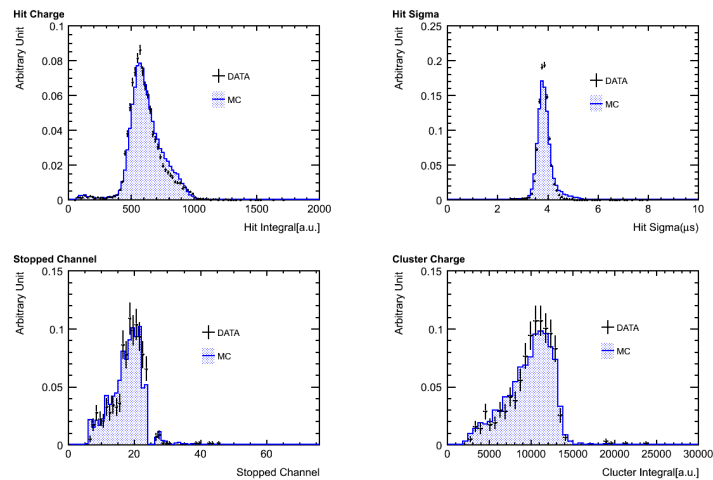


Figure 38: DATA-MC comparison of Hit Charge, Hit Sigma, Stopped Channel, Cluster Charge

the initial momentum.

Figure39 shows the integrated ADC distribution of each channel from stopped channel. The MC distribution of the channels after stopped channel are good agereements with DATA.

The left of figure40 shows the mean of the above distribution of each channel. The right of figure40 shows the ratios of DATA/MC. The ratios are suppressed within 94%~105%. From this result, we succeed in reproducing the charge response of DATA in high and wide dE/dx region.

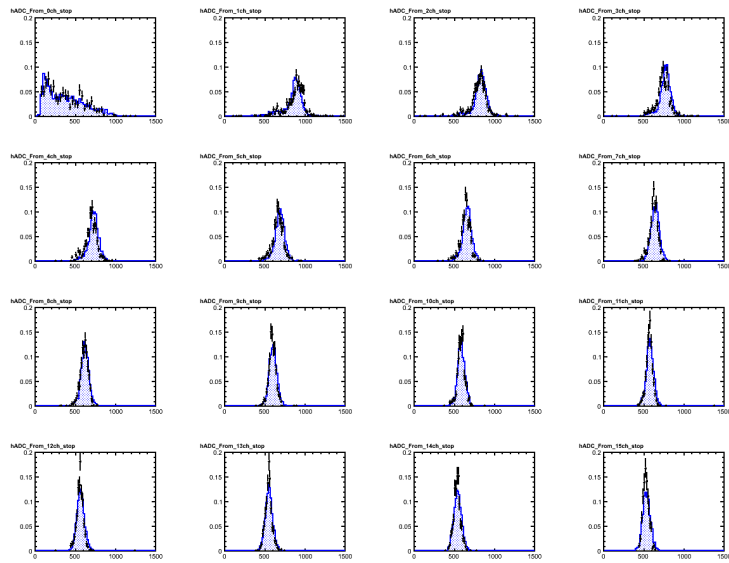


Figure 39: Integratedre ADC distribution of each channel from stopped channel

### 7.3. Recombination Factor

Electron-ion recombination depends on the electric field and stopping power  $dE/dx$ . We study this factor using tagged proton beam. Recombination factor measurement using proton beam is relatively easy because of stability of proton. This is why we used proton beam for this study as a first step.

Expression for recombination can be derived

$$Q = A \frac{Q_0}{1 + (k/E) \times (dE/dx) \times (1/\rho)} \quad (3)$$

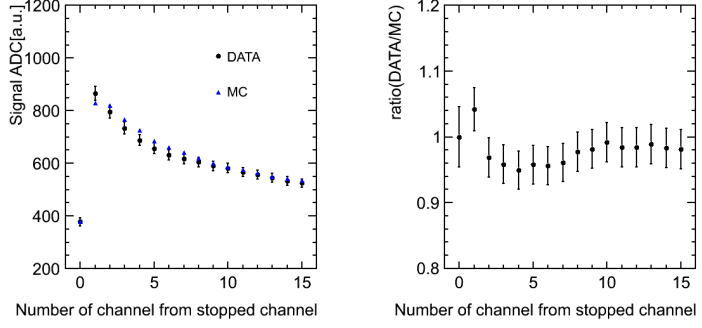


Figure 40: DATA-MC comparison of the mean of Integrated ADC distribution

where  $Q_0$  is initial ionization charge,  $E$  is electric field,  $dE/dx$  is energy deposit per distance,  $\rho$  is density of liquid Argon, A and k are fit parameters. This formula can be rearranged like below:

$$\frac{Q_0}{Q} = \frac{1}{A} + \frac{(k/E)(dE/dx)(1/\rho)}{A} \quad (4)$$

The ratio of  $Q_0/Q$  depends on stopping power  $dE/dx$ , so we determined fit parameter A and k using proton data and Monte Carlo simulation. In this analysis, we need  $Q$ ,  $Q_0$  and  $dE/dx$  channel by channel. First, electric field  $E$  was 200 V/cm in our test. Second,  $Q$  is integrated charge in an anode readout channel. Third,  $Q_0$  is integrated charge without recombination factor in an anode readout channel. And then,  $dE/dx$  per an anode channel is determined with truth information of Monte Carlo simulation. Figure 41, 42, 43 show  $Q$ ,  $Q_0$ ,  $dE/dx$  as a function of distance from stopped channel between 1 to 14 channel.  $Q$  is obtained from data,  $Q_0$  and  $dE/dx$  are obtained from Monte Carlo simulation. In many case, integrated charge in stopped channel are more affected by noise from next channel. This is the reason why we don't use information from stopped channel in this analysis.

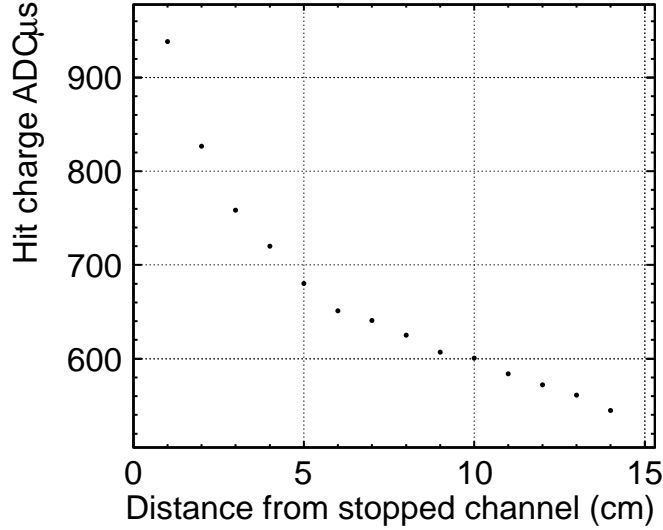


Figure 41: DATA:Integrated Flash ADC counts from stopped channel -1

The result of this study is shown in Fig44. Vertical axis is  $Q_0/Q$ , and horizontal axis is  $dE/dx$  in this figure, this plot is fitted by Birks law. As a result, we got fitting parameter

$$\begin{aligned} A &= 0.832 \pm 0.009(\text{stat.}) \pm 0.006(\text{syst.}) \\ k &= 0.0504 \pm 0.0010(\text{stat.}) \pm 0.0013(\text{syst.}) (\text{kV(g/cm}^2)/\text{cm/MeV}) \end{aligned} \quad (5)$$

We checked Birks law in the range  $4 \text{ MeV/(g/cm}^2) \leq dE/dx \leq 12 \text{ MeV/cm}^2$  and the result is consistent with ICARUS experiment's one[3] in – sigma.

#### 7.4. Stopped Kaon

In this section, we compare some quantities of data and MC simulation that K stops in the liquid argon detector and we can find stopped point. Figure 45 shows Data and MC comparison for signal hit charge, signal width, decay point and total particle charge distribution. Data of signal charge and signal width are consistent with MC one in error by less than two % and data of cluster charge and primary charge are consistent with MC one in error by less than five %.

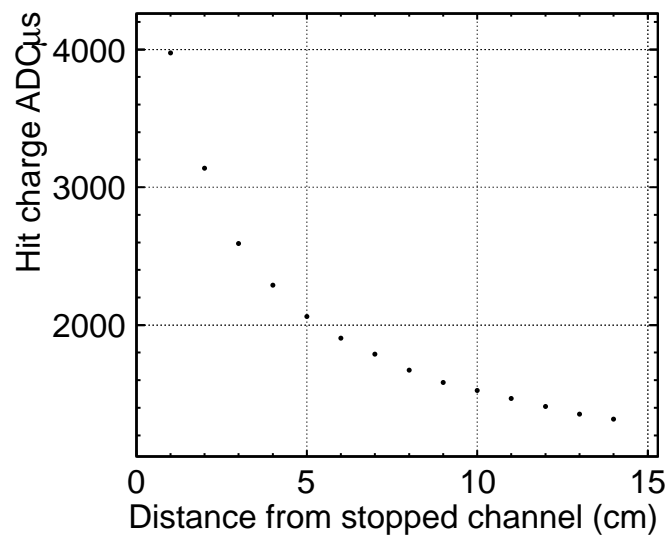


Figure 42: MC without recombination:Integrated Flash ADC counts from stopped channel -1

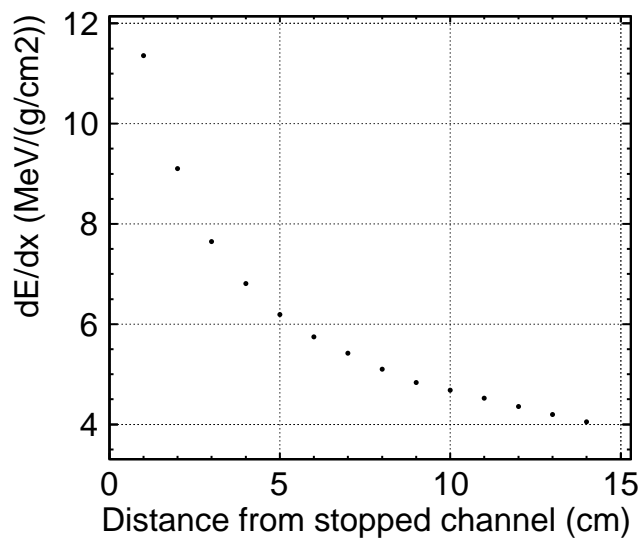


Figure 43:  $dE/dx$  from stopped channel -1

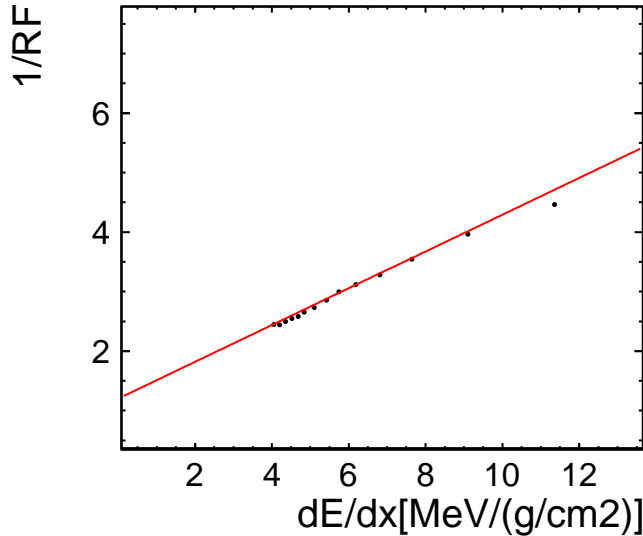


Figure 44: 1/RF VS  $dE/dx$ : fitted by Birks law

Figure 7.4 shows signal hit charge distribution of restricted channel 27. As shown in figure 7.4, signal charge have two peaks at 300 and 500 ADCus. Because two peaks has correlation of  $\Delta$ TOF, possible assumption of the cause is that beam line were bipolarized and the beam didn't pass in the center of the detector. So, we use only the event that signal charge of restricted channel 27 is less than 350. Figure 47 shows signal hit charge distribution in different distance from the stopped point.

As shown in figure 47, data is consistent with MC one. Figure 49 shows data/MC ratio of signal hit charge distribution in different distance from the stopped point. Data of signal charge in different distance from stopped point are consistent with MC one with in 5%.

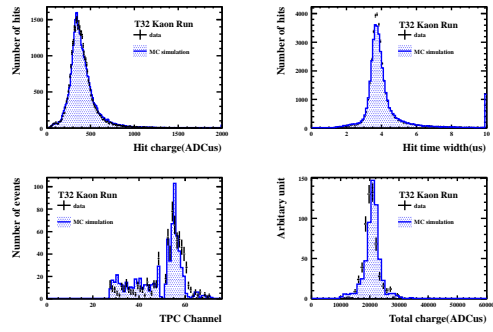


Figure 45: Data-MC comparison for hit charge, hit sigma, cluster charge, primary particle charge

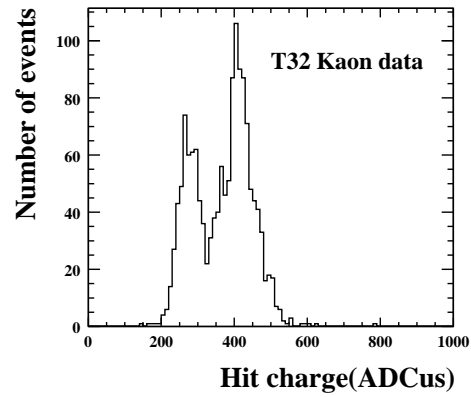


Figure 46: Hit charge in channel 27

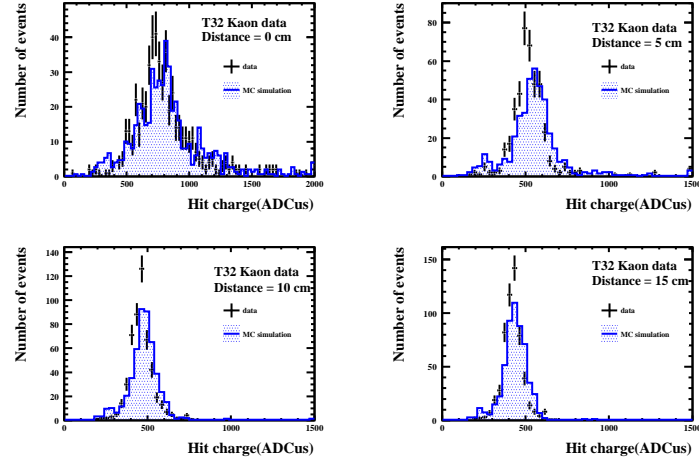


Figure 47: Data-MC comparison for hit charge distribution in different distance from the stopped point (top left: decay point, top right: decay point-5cm, bottom left: decay point-10cm, decay point-15cm)

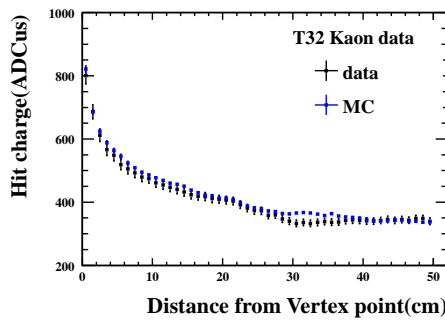


Figure 48: Data-MC comparison for hit charge distribution in different distance from the stopped point

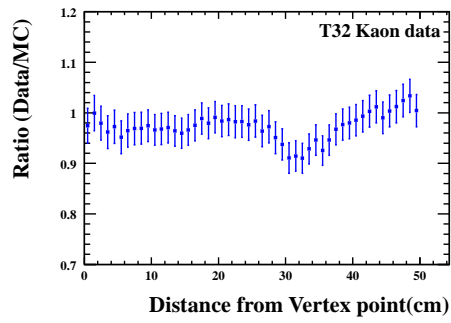


Figure 49: Data/MC ratio for hit charge distribution in different distance from the stopped point

## **8. Summary**

## References

- [1] O. Araoka *et al.*, J. Phys. Conf. Ser. **308**, 012008 (2011) [arXiv:1105.5818 [physics.ins-det]].
- [2] S. Mihara [MEG Collaboration], Nucl. Instrum. Meth. A **518**, 45 (2004).
- [3] S. Amoruso *et al.* [ICARUS Collaboration], Nucl. Instrum. Meth. A **523**, 275 (2004).
- [4] S. Amoruso, M. Antonello, P. Aprili, F. Arneodo, A. Badertscher, B. Baibusinov, M. Baldo-Ceolin and G. Battistoni *et al.*, Nucl. Instrum. Meth. A **516**, 68 (2004).
- [5] A. Bettini *et al.*, Nucl. Instrum. Meth. A **305**, 177 (1991).
- [6] P.V.C Hough 'Method and means for recognizing complex patterns', United States Patent Office 3069654(1962)